AFGL-TR-78-0046

STUDY TO DEVELOP GRADIOMETER TECHNIQUES

D. Schaechter
M. Kurosaki
D.B. DeBra

Stanford University
Guidance & Control Laboratory
Stanford, CA 94305

December 1977

Final Report
October 1976 - September 1977

AIR FORCE GEOPHYSICS LABORATORY
AIR FORCE SYSTEMS COMMAND
UNITED STATES AIR FORCE
HANSCOM AFB, MASSACHUSETTS 01731

SECURITY CLASSIFICATION OF THIS PAGE (When Data Entered)

REPORT DOCUMENTATION PAGE

READ INSTRUCTIONS BEFORE COMPLETING FORM

1 REPORT NUMBER (19) (12) AFGL-TR-78-0046	2 GOVT ACCESSION NO. / 3 RECIPIENT'S CATALOG NUMBER
4 TITLE (and Subtitle) (6) STUDY TO DEVELOP GRADIOMETER TECHNIQUES.	5 TYPE OF REPORT & PERIOD COVERED Final Report, Oct 1976 to Sep 1977
	6 PERFORMING ORG. REPORT NUMBER (14) 2-DBZ-7215
7 AUTHOR(s) (19) D. Schaechter, M. Kurosaki, D.B. DeBra, Principal Invs.	8 CONTRACT OR GRANT NUMBER(s) (15) F-19628-76-C-0289 NAS-2-1111
9 PERFORMING ORGANIZATION NAME AND ADDRESS Stanford University, Guidance & Control Lab., Dept. Aero and Astro, Stanford, Calif., 94305	10 PROGRAM ELEMENT, PROJECT, TASK AREA & WORK UNIT NUMBERS P.E. 63701B Work Unit No. 320103AC
11 CONTROLLING OFFICE NAME AND ADDRESS U.S. Air Force Geophysics Laboratory, (LWG) Hanscom AFB, Massachusetts, 01731 Monitor, James A. Hammond	12 REPORT DATE (11) Dec 1977 / 13 NUMBER OF PAGES 58
14 MONITORING AGENCY NAME & ADDRESS (if different from Controlling Office)	15 SECURITY CLASS. (of this report) unclassified / 15a DECLASSIFICATION/DOWNGRADING SCHEDULE

16 DISTRIBUTION STATEMENT (of this Report)

Approved for public release. Distribution Unlimited.

17 DISTRIBUTION STATEMENT (of the abstract entered in Block 20, if different from Report)

18 SUPPLEMENTARY NOTES

19 KEY WORDS (Continue on reverse side if necessary and identify by block number)

gravity gradiometry/gradiometers, tesseral harmonics, bias estimation, Kalman filter, geodesy, inertial navigation, deflection (gravity, vertical, etc)

20 ABSTRACT (Continue on reverse side if necessary and identify by block number)

The primary goal of the current gravity gradiometer research at Stanford has been to establish the feasibility of using a gravity gradiometer with 1 E accuracy, as the primary sensor in various applications. The two applications considered here in detail are geodesy missions and inertial navigation systems. Preliminary sections on gravity models and gravity gradiometer bias estimation are also included.

DD FORM 1 JAN 73 1473 EDITION OF 1 NOV 65 IS OBSOLETE S/N 0102 LF 014 6601

SECURITY CLASSIFICATION OF THIS PAGE (When Data Entered)

STUDY TO DEVELOP GRADIOMETER TECHNIQUES

I. INTRODUCTION

There are three moving base gravity gradiometers currently under development. The instruments are being developed at Hughes Research Labs [Ref. 1], the Bell Aerospace Corp. [2], and the Charles Stark Draper Lab. [3, 4]. The design goal for each of the sensors is 1 Eötvös. Furthermore, 0.1 Eötvös (E) accuracy should be feasible from an orbiting gravity gradiometer [5]. The group of instruments includes sensors designed specifically to measure the gravity gradient, as well as sensors, which utilize existing accelerometers to provide a gradient estimate. The Hughes and Bell instruments rotate, thus modulating the information. This rotation transfers the gravity gradient signal to a higher frequency, quieter part of the spectrum, and can separate the signal from some sources of instrument bias. The Draper Lab sensor measures the gradient signal at zero frequency and uses a sophisticated flotation suspension system to isolate the sensing element from errors induced by rotation and jitter. A system of at least three instruments of any one type is required in order to provide a complete gravity gradient tensor estimate. Often times, however, it is possible to extract all the information that is required from a single one of these instruments.

The primary objectives of this paper, oriented toward the use of a workable gravity gradiometer as a sensing element in several applications, are given below:

1) To develop models for gravity gradient anomalies and gravity anomalies,

2) To evaluate several methods of on-line instrument bias estimation,

3) To determine the performance of a gradiometer in mapping the earth's gravity field,

4) To assess inertial navigation systems augmented with a gravity gradiometer.

The work under this contract, and the work under a separate contract (Goddard SFC — NAS 5-21960) to evaluate the performance of a geodesy mission with orbiting gradiometers have some overlap, especially in the groundwork areas of instrument performance and capability, and gravity models. As such, we hope it will be valuable to supply some results from work performed under that contract in this Final Report.

Chapter II

GRAVITY AND GRAVITY GRADIENT MODELS

In order to evaluate the capability of gravity gradiometers, or systems in which the gravity gradiometer is an essential component, some model of the type of inputs is required. Several of the models are:

1) tesseral harmonic models using Kaula's rule [7] ,

2) tesseral harmonic models using Allan's rule [8] ,

3) point mass and line mass models,

4) experimentally determined second-order random process models.

Once a given model is chosen, the gravitational potential, force, and gradient can be ascertained. The choice of which model is to be used in a given implementation depends on the dynamic range of interest for a given system (which is in turn dependent on the system's speed relative to the earth). This can vary substantially, from fixed base application, to ship speed, airplane speed, and finally, orbital speed. The various models also result in different degrees of complexity. This, too, must be considered for any mechanization involving gravity gradiometers.

This chapter contains the expressions for the gravity forces and gradients, and their correlation based on various gravity models.

A. TESSERAL HARMONIC MODELS

The most general expression of an arbitrary function over the surface of a sphere that satisfies the potential equation is in terms of tesseral harmonics. The tesseral harmonic expansion of the earth's gravitational potential is

$$V(r,\varphi,\lambda) = \frac{\mu_\oplus}{r}\left\{1 - \sum_{\ell}\sum_{m=1}^{\ell}\left(\frac{R_\oplus}{r}\right)^{\ell} \bar{P}_{\ell m}(\sin\varphi)\left[\bar{C}_{\ell m}\cos m\lambda + \bar{S}_{\ell m}\sin m\lambda\right]\right\}, \tag{1}$$

where (r,φ,λ) is the position of a test point in terms of the spherical coordinates, radius, latitude, and longitude; $\mu_\oplus = GM_\oplus$; $R_\oplus$ = radius of the earth; $\bar{P}_{\ell m}(x)$ are normalized associated Legendre polynomials, and $\bar{C}_{\ell m}$ and $\bar{S}_{\ell m}$ are normalized tesseral harmonic coefficients, which give the amount of each harmonic present; the perturbation potential due to a particular harmonic is simply

$$V_{\ell m} = \frac{\mu_\oplus}{r}\left(\frac{R_\oplus}{r}\right)^{\ell} \bar{P}_{\ell m}(\sin\varphi)\,\bar{J}_{\ell m} \tag{2}$$

where

$$\bar{J}_{\ell m} = \sqrt{\bar{S}_{\ell m} + \bar{C}^2_{\ell m}}$$

and in writing (2), the phase information is lost.

Estimates of the magnitudes of the $\bar{J}_{\ell m}$'s are given by Kaula [7] and Allan [8]. Kaula's familiar rule of thumb for $\bar{J}_{\ell m}$ is

$$\bar{J}_{\ell m} \sim \frac{\sqrt{2}\ 10^{-5}}{\ell^2} \tag{3}$$

while Allan's more complicated formula is

$$\bar{J}_{\ell m} \sim \frac{\sqrt{12.2 \times 10^{-10}}\,(0.93)^{\ell+3/2}}{(2\ell+1)\sqrt{2\ell+3}} \tag{4}$$

Although, different in form, both formulas agree quite closely over huge ranges of the subscript ℓ, and with measured values of the tesseral harmonic coefficients.

With estimates of the magnitudes of the $\bar{J}_{\ell m}$ in (3) and (4), it becomes possible to estimate the magnitude of the perturbation potential $V_{\ell m}$, and hence of the force $(\vec{f})$ and gradient $(\vec{\vec{f}})$ perturbations, since

$$\vec{f} = \frac{\partial V}{\partial \vec{r}} \tag{5a}$$

and

$$\vec{\vec{\Gamma}} = \frac{\partial \vec{f}}{\partial \vec{r}} \quad . \tag{5b}$$

If we further assume that the phases of the harmonics are random, it becomes possible to obtain closed-form approximate expressions for the variance of the perturbation forces, the variance of the perturbation gravity gradient, and the covariance of the perturbation forces and gradients due to the tesseral harmonics.

The total variance of the force is computed for a representative force component (f_r) via Kaula's rule. It is given by

$$\sigma_f^2 = E(f_r^2) = \sum_{\ell} (f_{r_\ell})^2 \ell \ (m \sec^2)^2 \tag{6}$$

where f_{r_ℓ} is the radial force perturbation due to the ℓth harmonic. The extra ℓ in (6) is due to the fact there are ℓ distinct harmonics ($m = 1$ to ℓ) for a particular ℓ.

f_r is obtained as the radial derivative

$$f_{r_\ell} \sim -\ell \frac{\mu_\oplus}{r^2} \left(\frac{R_\oplus}{r}\right)^2 \bar{P}_{\ell m}(\sin \varphi) \bar{J}_{\ell m} \tag{7a}$$

so

$$f_{r_\ell} \sim -\ell \, g\left(\frac{R_\oplus}{r}\right)^{\ell+2} \bar{P}_{\ell m}(\sin \varphi) \bar{J}_{\ell m} \tag{7b}$$

since

$$\frac{\mu_\oplus}{r^2} = g\left(\frac{R_\oplus}{r^2}\right)$$

where g is the gravitational acceleration at the surface of the earth.

Squaring (7), inserting it into (6), using that $\bar{P}^2_{\ell m}(\sin \varphi)\big|_{avg} = 1$ by definition, and using Kaula's rule for $\bar{J}_{\ell m}$, we obtain

$$\sigma_f^2 \quad E(f_r^2) \;=\; 2 \times 10^{-10}\, g^2 \left(\frac{R_\oplus}{r}\right)^4 \sum_{\ell \geq 2} \frac{1}{\ell} \left(\frac{R_\oplus}{r}\right)^{2\ell} \tag{8a}$$

so

$$\sigma_f = \sqrt{2} \times 10^{-5}\, g \left(\frac{R_\oplus}{r}\right)^2 \sqrt{\log \frac{1}{1 - \left(\frac{R_\oplus}{r}\right)^2} - \left(\frac{R_\oplus}{r}\right)^2} \quad . \tag{8b}$$

An identical approach leads to closed-form expression for the gradients. There

$$\Gamma_{rr} \quad n^2 \ell 2 \left(\frac{R_\oplus}{r}\right)^\ell \bar{P}_{\ell m} (\sin \phi)\, \bar{J}_{\ell m}$$

where $n^2 = \mu_\oplus / r^3$. Using

$$\sigma_\Gamma^2 \;=\; E(\Gamma_{rr}^2) \;=\; \sum_\ell (\Gamma_\ell rr)^2 \cdot \ell \quad , \tag{9}$$

eventually, using Kaula's rule,

$$\sigma_\Gamma^2 \;=\; 2 \times 10^{-10}\, n^4 \sum_{\ell \geq 2} \ell \left(\frac{R_\oplus}{r}\right)^{2\ell} \tag{10}$$

so

$$\sigma_\Gamma \;=\; \sqrt{2} \times 10^{-5}\, n^2 \frac{\left(\frac{R_\oplus}{r}\right)^2 \sqrt{2 - \left(\frac{R_\oplus}{r}\right)^2}}{1 - \left(\frac{R_\oplus}{r}\right)^2} \quad .$$

Substitution of Allan's rule (4) into (9) gives a slightly more cumbersome series to sum. The results are

$$\sigma_f^2 \;=\; \frac{12.2 \times 10^{-10}}{8(0.93)}\, g^2 \sum_{\ell \geq 2} \left(0.93 \frac{R_\oplus}{r}\right)^{2\ell+4} \tag{11}$$

so

$$\sigma_f \;=\; 1.28 \times 10^{-5}\, g \frac{x^2}{\sqrt{1 - x}}$$

where

$$x \;=\; \left(0.93 \frac{R_\oplus}{r}\right)^2 \quad .$$

Similarly

$$\sigma_\Gamma^2 = \frac{12.2\times10^{-10}}{g}(0.93)^3 n^4 \sum_{\ell\geq 2} \ell^2 \left(0.93\frac{R_\oplus}{r}\right)^{2\ell} \qquad (12)$$

so

$$\sigma_\Gamma = 1.11\times10^{-5}\, n^2 \frac{x^2(4 - 3x + x^2)}{(1 - x)^3}$$

where

$$x = \left(0.93\frac{R_\oplus}{r}\right)^2 .$$

The results of Eqs. (8), (10), (11), and (12) are plotted in Fig. 1. It shows the standard deviation of the force perturbations and gradient perturbations at various altitudes. Figure 1 also shows that as the test point approaches the earth's surface, the standard deviation of the gradient using Kaula's rule blows up, a phenomena that physically does not occur. Although Kaula's rule is in common use, it evidently does not attenuate the high frequency components rapidly enough to produce a finite standard deviation at the surface. Allan's rule does provide for a more rapid attenuation of the high frequency components, due to the presence of the $(0.93)^\ell$ term in (4), and does result in finite force and gradient variances.

One useful feature of the closed-form solutions of the standard deviations is the ability to determine what amount of variance is due to different portions of the spectrum. A particularly simple example is obtained from the force components in (11). The analytical expression for σ_f due to harmonics above some degree k is easily found to be $1.28 \times 10^{-5} g \sqrt{x^{k+2}/1 - x}$ where again $x = 0.93(R_\oplus/r)^2$. Near the surface of the earth, then, the percent of variance contribution due to harmonic degree greater than or equal to k is given as

$$\frac{\frac{x^{k+2}}{1 - x}}{\frac{x^2}{1 - x}} = x^k$$

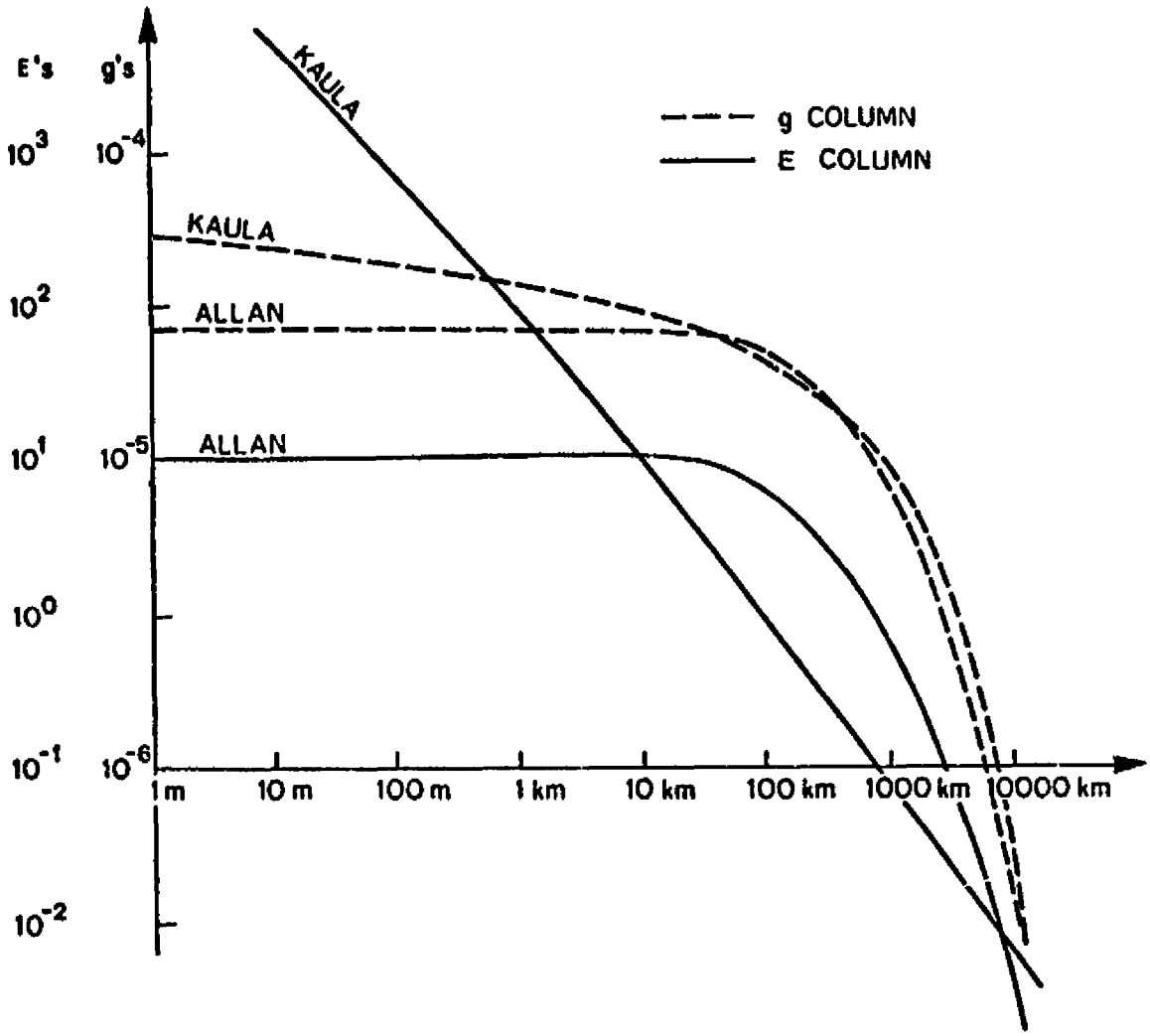

Solid line is Eötvös units column or ordinate.
Dash line is g column or ordinate.

FIG. 1 1 σ VALUES FOR FORCE AND GRADIENT PERTURBATIONS.

where $x \approx (0,93)^2$. In order to account for only 50% of the noise, a model of fifth degree (~ 30 coefficients!) is required, for 75% of the noise 10th (~110 coefficients) degree, etc. The gradient components attenuate even less rapidly requiring an even higher order model. This certainly proves that an improved tesseral harmonic model of the earth is <u>not</u> the way to go in order to improve navigator accuracy due to the high degree of the model required to give even modest improvement.

In order to compare results of other models to this model, the correlation coefficients for $\Gamma_{r\varphi}$ and g_{φ}, and for $\Gamma_{rr} - \Gamma_{\varphi\varphi}$ and g_r were computed on the basis of the tesseral harmonic model with random phases. These correlation coefficients are given below near the earth's surface

$$\frac{E(\Gamma_{r\varphi},\ g_{\varphi})}{\sqrt{[E(\Gamma_{r\varphi}^2)][E(g_{\varphi}^2)]}} = +0.63$$

and

$$\frac{E(\Gamma_{rr} - \Gamma_{\varphi\varphi},\ g_r)}{\sqrt{[E(\Gamma_{rr} - \Gamma_{\varphi\varphi})^2][E(g_{\varphi}^2)]}} = -0.63.$$

B. POINT MASS AND LINE MASS MODELS

The point mass and line mass models approximate local gravity anomalies much better than the tesseral harmonic model which has primary use in describing global features.

A simplified analysis of a point disturbance begins with the assumption of a point mass with mass m_d, $\mu_d = Gm_d$, and a local 2-D x, y coordinate frame as is shown in Fig. 2.

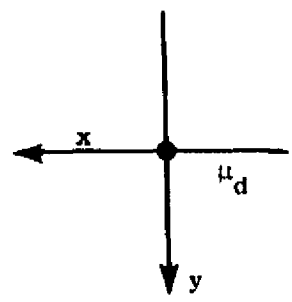

FIG. 2 POINT MASS MODEL

The disturbance potential due to μ_d at a point (x, y) is simply $V = -\mu/r = \mu\sqrt{x^2 + y^2}$. Expressions for the forces and gradients are easily obtained by taking the respective partial derivatives,

$$f_x = \frac{\mu x}{r^3}\ ; \qquad f_y = \frac{\mu y}{r^3}\ ;$$

$$\Gamma_{xx} - \Gamma_{yy} = \frac{3\mu(-x^2 + y^2)}{r^5}\ ; \quad 2\Gamma_{xy} = -\frac{6\mu xy}{r^5} \tag{13}$$

where $r = \sqrt{x^2 + y^2}$.

The correlation between the four quantities in (13) can be found by assuming each of them is an independent measurement, and that the measurements are obtained along a prescribed path in the x, y plane. For simplicity, the path chosen here is the path y constant, and x proceeds from $-\infty$ to $+\infty$ at a constant rate (the path an airplane might follow). The information matrix is then given by

$$I = \int \begin{bmatrix} f_x \\ f_y \\ \Gamma_{xx} - \Gamma_{yy} \\ \Gamma_{xy} \end{bmatrix} [f_x,\ f_y,\ \Gamma_{xx}-\Gamma_{yy},\ \Gamma_{xy}]dx \tag{14}$$

and the covariance matrix P is simply I^{-1}. Normalized off-diagonal elements of P give the correlation coefficients. A typical integration is shown below

$$I_{11} = \int_{-\infty}^{\infty} f_x^2 dx = \int_{-\infty}^{\infty} \frac{x^2 dx}{(x^2+y^2)^3} = \int_{-\pi/2}^{\pi/2} \frac{y^2\tan^2\theta(y\ \sec^2\theta d\theta)}{y^6\ \sec^6\theta}$$

$$I_{11} = \frac{1}{y^3}\int_{\pi/2}^{\pi/2} \tan^2\theta\ \cos^4\theta d\theta = \frac{\pi}{y^3}\left(\frac{1}{8}\right)\ . \tag{15}$$

Evaluating every element of I

$$I = \begin{bmatrix} \frac{\pi}{y^3}\frac{1}{8} & 0 & 0 & -\frac{\pi}{y^4}\frac{3}{8} \\ 0 & \frac{\pi}{y^3}\frac{3}{8} & \frac{\pi}{y^4}\frac{1}{4} & 0 \\ 0 & \frac{\pi}{y^4}\frac{1}{4} & \frac{9\pi}{y^5}\frac{7}{32} & 0 \\ -\frac{\pi}{y^4}\frac{3}{8} & 0 & 0 & \frac{9}{y^5}\frac{5}{32} \end{bmatrix} \qquad (16)$$

Normalizing I, and reordering rows and columns

$$I = \left[\begin{array}{cc:cc} 1 & -2 & 0 & 0 \\ -2 & 5 & 0 & 0 \\ \hdashline 0 & 0 & 3 & 4 \\ 0 & 0 & 4 & 7 \end{array}\right] \begin{matrix} f_x \\ 2\Gamma_{xy} \\ f_y \\ \Gamma_{xx}-\Gamma_{xy} \end{matrix} \qquad (17)$$

$$\begin{matrix} f_x & 2\Gamma_{xy} & f_y & \Gamma_{xx}-\Gamma_{xy} \end{matrix}$$

From (17) it is found that Γ_{xy} is highly correlated with f_x (and with nothing else) with correlation coefficient $2/\sqrt{5} = 0.895$, and also that $\Gamma_{xx} - \Gamma_{yy}$ is highly correlated with f_y (and with nothing else) with correlation coefficient $-4/\sqrt{21} = -0.875$.

This nearly perfect correlation has particular significance for gravity gradiometer system implementations. In most cases, the gravity gradiometer is used as a sensor to provide force perturbations due to gravity anomalies that the accelerometers cannot provide and that contain too much high frequency information for an a priori earth gravity model to approximate. Instead of proceeding along the path of integrating the gradient information to give the forces (which leads to problems if the gradiometer measurement contains a bias), the correlation of the forces

with the gradients gives a way of proceeding directly from the gradients to the forces without augmenting the states of the system. In fact, from (16) we obtain

$$f_x \sim \sqrt{\frac{\frac{\pi}{3}\frac{1}{8}}{\frac{36\pi}{y^5}\frac{5}{16}\frac{3}{8}}} \quad (2\Gamma_{xy}) = \frac{y}{6}\sqrt{\frac{16}{5}} \quad (2\Gamma_{xy})$$

$$f_x \sim 0.3y \ (2\Gamma_{xy})$$

and

$$f_y \sim -\sqrt{\frac{\frac{\pi}{3}\frac{3}{8}}{\frac{9\pi}{y^5}\frac{7}{32}}} \ (\Gamma_{xx} - \Gamma_{yy}) = -y\sqrt{\frac{4}{21}} \ (\Gamma_{xx} - \Gamma_{yy})$$

$$f_y \sim -0.43y \ (\Gamma_{xx} - \Gamma_{yy})$$

where y is a correlation height or a mean height of the vehicle above the disturbances. A simple gain adjustment is all that is needed then to provide the force perturbations from the gradient information.

B. LINE MASS MODELS

The line mass model is another possible alternate to locally modeling gravitational perturbations. To determine if line mass models or point mass models result in better performance will require surveying data to discover if local gravity perturbations are more accurately modeled with line masses or point masses. Surprisingly, the use of point masses vs line masses produces relatively minor differences. The line mass model is shown in Fig. 3.

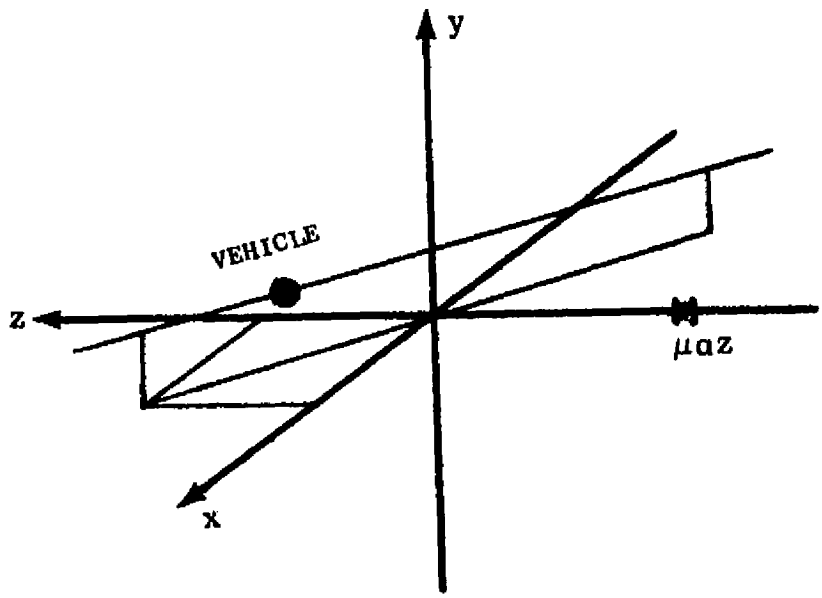

FIG. 3 LINE MASS MODEL

The disturbance potential V is simply

$$V = -2 \int_0^\infty \frac{\mu dz}{(x^2+y^2+z^2)^{\frac{1}{2}}} = -2 \int_0^\infty \frac{\mu dz}{r} \qquad (18)$$

where now μ is a mass per unit length. (Note that V in (18) is independent of z.) Expressions for the force and gradient expression are again obtained

$$
\begin{aligned}
f_x &= 2\int_0^\infty \frac{\mu x\, dz}{r^3} \\
f_y &= 2\int_0^\infty \frac{\mu y\, dz}{r^3} \\
2\Gamma_{xy} &= 4\int_0^\infty \frac{-3xy\ \mu dz}{r^5} \\
\Gamma_{xx}-\Gamma_{yy} &= 2\int_0^\infty \frac{(3y^2 - 3x^2)\mu dz}{r^5} \quad .
\end{aligned}
\tag{19}
$$

The correlation between the various elements is obtained by the procedure described in (14) and (15). The identical substitutions are made here as in the point mass model, the integrations carried out, and the results are that Γ_{xy} is correlated with f_x (and with nothing else) with correlation coefficient $1/\sqrt{2} = 0.71$ and that $\Gamma_{xx} - \Gamma_{yy}$ is correlated with f_y (and with nothing else) with correlation coefficient $-1/\sqrt{2} = -0.71$. Although the correlation is not as strong as with the point mass models, it is still quite high. Perhaps it is appropriate in the final model, to actually use a correlation coefficient between the values given by line mass models and point mass models. Again, scale heights can be derived to relate directly the gradient perturbations with the force perturbations.

An obvious advantage of these correlation models over dynamic models of the earth's gravity gradient perturbations, deflections of the vertical, and perturbation force components, is the simplicity. A dynamic model involves earth surveying to "fit" parameters in the model, which may themselves vary substantially over different regions of the earth. An added advantage is that the correlation models do not involve "augmenting the state" of the system, as do the dynamic models.

Chapter III
BIAS ESTIMATION

Regardless of the eventual use of the gravity gradiometer, some type of signal processing will be required to minimize the effects of one of the largest gravity gradiometer errors: an unknown instrument bias. As will be discussed in Chapter V, a gradiometer bias has the same effect as a gyroscope drift when used in an inertial navigator, i.e., they both produce unbounded position errors with increasing time. When the gradiometer is used as the sensor to perform geodesy experiments from orbit, the gradiometer bias produces a bias in the estimate of the dominant term of the earth's gravity field.

This Chapter contains a study of several attempts to eliminate the gravity gradiometer bias error.

One greatly simplified model of the bias estimation problem is given below. A single (rotating) gradiometer supplies two pieces of information of the gravity gradient at a point, the difference of two principal elements of the gravity gradient tensor and one diagonal component. For example,

$$\begin{aligned} z_1 &= x_{11} - x_{22} \\ z_2 &= x_{12} \,. \end{aligned} \tag{20}$$

A set of three such gradiometers pointing in orthogonal directions along with Laplace's constraint equation (that the sum of the diagonal elements equal zero) is sufficient to determine the gravity gradient at a point; i.e., the problem below:

$$
\begin{aligned}
z_1 &= x_{11} - x_{22} \\
z_2 &= x_{12} \\
z_3 &= x_{22} - x_{33} \\
z_4 &= x_{23} \\
z_5 &= x_{33} - x_{11} \\
z_6 &= x_{13} \\
z_7 &= x_{11} + x_{22} + x_{33} = 0
\end{aligned}
\qquad \text{or} \quad z = Hx \qquad (21)
$$

is invertible, and hence solvable for x in terms of z. (It is not invertible without the constraint equation z_7.) In fact, $\hat{x} = (H^T H)^{-1} H^T z$. Even if random noise v_i with covariance r_i is inserted into each of the first six equations in (21), it is possible to obtain a least-squares estimate for x in terms of z. In fact, $\hat{x} = (H^T R^{-1} H)^{-1} H^T R^{-1} z$ and the variance of the estimate error $P = (H^T R^{-1} H)^{-1}$. Since z_7 is an "exact" measurement though, either infinitesimal values for the corresponding element of R must be used and a limit process applies or else the matrix inversion lemma [10] may be used. The matrix inversion lemma can yield the improved covariance matrix P from the covariance matrix P'. P' is the easily computed covariance matrix which does not include the beneficial effects of the exact constraint equation. The formula relating P to P' is

$$P = P'\bar{H}^T(\bar{H}P'\bar{H}^T)^{-1}\bar{H}P'$$

where H reflects the constraint equation structure that

$$x_{11} + x_{22} + x_3 = 0 = \bar{H}x$$

so

$$\bar{H} = [1 \quad 1 \quad 1 \quad 0 \quad 0 \quad 0] .$$

The advantage of the matrix inversion lemma procedure is that it completely avoids the limiting processes mentioned earlier.

Now consider the problem of augmenting the state vector with constant but unknown biases, 1 bias per gradiometer. Now

$$
\begin{aligned}
z_1 &= x_{11} - x_{22} + b_1 \\
z_2 &= x_{12} + b_1 \\
z_3 &= x_{22} - x_{33} + b_2 \\
z_4 &= x_{23} + b_2 \\
z_5 &= x_{33} - x_{11} + b_3 \\
z_6 &= x_{13} + b_3 \\
z_7 &= x_{11} + x_{22} + x_{33} = 0
\end{aligned}
\qquad z = H' \left[\begin{array}{c} x \\ \hline b \end{array}\right] \qquad (23)
$$

and although the sum of the biases $b_1 + b_2 + b_3$ is obtainable (from $z_1 + z_2 + z_3 - z_7$), it is impossible to obtain any other combination of the biases (in particular, the individual biases) and, therefore, it is impossible to solve for x.

The only useful results from (23) are obtained if there is some a priori estimate of the biases. In this case, the usual Kalman filter techniques will allow for estimates of x to be obtained from noisy measurements, however the conditioning of the problem is of course dependent on the initial accuracy of b. If I_0 is the initial information on the augmented state ($P_0 = I_0^{-1}$), then the update equations are simply

$$
\begin{aligned}
\hat{x}_1 &= \hat{x}_0 + (I_1)^{-1} H'^T R^{-1} z \\
I_1 &= I_0 + H'^T R^{-1} H'
\end{aligned}
\qquad (23)
$$

where H' is the measurement matrix for the augmented state vector,

and R the covariance of the measurement accuracy.

The advantage of the initial information, I_0, is evident in the second equation of (23). Whereas $H'^T R^{-1} H'$ is not invertible, the sum $I_0 + H'^T R^{-1} H'$ is invertible and hence the inverses appearing in the estimate update equation are valid.

More sophisticated schemes for estimating the biases make use of dynamic models of the system, as opposed to the model in which both the gradient components and the biases were constants. Of course, since an a priori model of either the measurement or the state presumes additional information is available, it should be expected that better results could be obtained at the expense of additional complexity.

Two additional bias estimation schemes will be discussed. The first makes use of the fact that the bias is fixed in the instrument frame, while what the gradiometer measures will generally be fixed in an inertial frame. Rotating the spin axis of the gradiometer should then distinguish between the gradient components and the bias terms. The second method again distinguishes between the gradient components and the bias terms but now, the mechanism is via a model of the gradient perturbations. This is where much of the material from Ch. I can be used.

Beginning first with the rotation scheme, an expression for $\vec{\vec{\Gamma}}$, the gradient tensor is

$$\vec{\vec{\Gamma}} = \begin{bmatrix} \Gamma_{11} & \Gamma_{12} & \Gamma_{13} \\ \Gamma_{12} & \Gamma_{22} & \Gamma_{23} \\ \Gamma_{13} & \Gamma_{23} & \Gamma_{33} \end{bmatrix}$$

Assuming the gravity gradiometer spin axis is rotated about the 1 axis

$$\vec{\vec{\Gamma}} = T \vec{\vec{\Gamma}} T^T$$

where

$$T = \begin{bmatrix} 1 & 0 & 0 \\ 0 & \cos(\omega t) & \sin(\omega t) \\ 0 & -\sin(\omega t) & \cos(\omega t) \end{bmatrix}$$

and ω is the rotation frequency.

Then a single gradiometer, capable of measuring (say, without loss of generality) the $\Gamma_{11} - \Gamma_{22}$ and Γ_{12} components would output

$$z_1 = \Gamma_{11} - (\Gamma_{22} \cos^2\omega t + 2\Gamma_{23} \sin \omega t \cos \omega t + F_{33} \sin^2\omega t) + b_1 + v_1 ;$$

$$z_2 = \Gamma_{12} \cos \omega t + \Gamma_{13} \sin \omega t + b_2 + v_2$$

where b_1 and b_2 are biases, and v_1 and v_2 are random noise. Now

$$z = H \left[\frac{x}{b}\right]$$

and H is time varying. In fact

$$\begin{bmatrix} z_1 \\ z_2 \\ z_3 \end{bmatrix} = \begin{bmatrix} 1 & -\cos^2\omega t & -\sin^2\omega t & 0 & 0 & 2\sin \omega t \cos \omega t & 1 & 0 \\ 0 & 0 & 0 & \cos \omega t & \sin \omega t & 0 & 0 & 1 \\ 1 & 1 & 1 & 0 & 0 & 0 & 0 & 0 \end{bmatrix} \begin{bmatrix} \Gamma_{11} \\ \Gamma_{22} \\ \Gamma_{33} \\ \Gamma_{12} \\ \Gamma_{13} \\ \Gamma_{23} \\ b_1 \\ b_2 \end{bmatrix} + \begin{bmatrix} v_1 \\ v_2 \end{bmatrix} \quad (24)$$

Again we have the constraint equation, $z_3 = \Gamma_{11} + \Gamma_{22} + \Gamma_{33} = 0$. Note that for $t = 0$, the time-varying H in (24) agrees with the H in (23).

The standard test for observability can be performed on the matrix H in (24) to determine the maximal rank of the matrix

$$\mathcal{O} = \begin{bmatrix} H \\ \dot{H} \\ \ddot{H} \\ \vdots \end{bmatrix} .$$

It turns out that the maximal rank of $\mathcal{O}$ is 7, so one mode is still not observable. Additional algebra yields the result that the mode $b_1 - \Gamma_{11}$ is not observable, but that $2/3\, b_1 + \Gamma_{11}$ is observable. What this says is that it is still not possible to distinguish between Γ_{11} and b. This result is easily explainable since the gradiometer spin axis never has a vertical component with the single axis rotation scheme we have considered here. However, if a two axis rotation scheme where the spin axis of the gradiometer spans all directions, all the parameters are observable, and hence the gradient components and individual biases are obtainable from z.

A problem with the continuous rotation schemes yet to be discussed is the introduction of a gradient field due to the kinematics of the rotation itself. The vector formula for this induced gradient field is

$$\vec{\Gamma}_{\omega} = \frac{d}{d\vec{r}} [\vec{\omega} \times (\vec{\omega} \times \vec{r})] = \vec{\omega}\vec{\omega} - \hat{I}\omega^2. \qquad (25)$$

In two dimensions the gradient field reduces to simply ω^2. If the spin axis rotates as slowly as $2\pi/50$ sec, the required accuracy of this rotation rate to obtain full potential of the fixed instrument accuracy is ~ 1 part in 10^{-9} ! Since this accuracy is not feasible, the continuous rotation schemes are ruled out.

Still, some use can be made of the preceding analysis. The fact that all the states and biases are observable with the continuous two axes rotation scheme means that with a sufficient number of discrete measurement points, the same information will be available. This can be accomplished in several ways. One scheme is to "calibrate" the gravity gradiometer at a fixed position, in several orientations to obtain the bias. If the bias is truly constant, the unit could then be used at new locations with the predetermined value of the bias. A second scheme is to simply repeat measurements with a moving base gravity gradiometer with the instrument oriented in different directions. For example, in a surveying mission, either with an airplane or satellite, it is possible to retrace a groundtrack while making measurements in (three) different orientations. This determines the bias and states on-line, in which case the effects of bias drift could be minimized.

The second scheme for distinguishing the gradient components from the biases is via a dynamic model of the gradient components. A simplification of a model to appear in a later chapter appears below. Again, letting x denote the gradient components, a linear dynamic model of x would be $\dot{x} = Fx + \Gamma w$ where w is a random process. Since $\dot{b} = 0$, there is again a mechanism for distinguishing x and b. Adjoining b to x

$$\begin{bmatrix} \dot{x} \\ \hline \dot{b} \end{bmatrix} = \underbrace{\left[\begin{array}{c|c} F & 0 \\ \hline 0 & 0 \end{array}\right]}_{F'} + \underbrace{\begin{bmatrix} \Gamma \\ \hline 0 \end{bmatrix}}_{\Gamma'} w$$

$$z = H \begin{bmatrix} x \\ \hline b \end{bmatrix} + v$$

$$E(vv^T) = R$$

$$E(ww^T) = Q \, .$$

$$\dot{I} = -IF' - F'^T I + H^T R^{-1} H - I\Gamma' Q \Gamma'^T I \, . \qquad (26)$$

As before, even though $H^T R' H$ in (26) is not invertible for use in the estimate update equation, the sum of the terms on the right-hand side of (26) is, and so eventually, it will be possible to distinguish x from b. More on the use of a model of the earth gravity field with applications to initial navigation will appear later.

Chapter IV

GEODESY

Several experiments have emerged which have the capability of very accurately measuring the gravitational field of the earth. These geodesy experiments which measure the higher harmonics of the earth include (1) high-low and low-low satellite-to-satellite (S-S) tracking; (2) counter-orbiting (C,O) drag-free satellites; (3) altimeter measurements from orbit; (4) orbiting gravity gradiometer measurements; (5) others.

The purpose of this chapter is to determine the accuracy to which the higher harmonics of the earth's gravity field could be deduced with an orbiting gravity gradiometer, and to compare these results with some of the previously mentioned experiments.

The starting point is to expand the earth's gravity field in a series of tesseral harmonics. Recall from (1) the usual representation of the perturbation potential as

$$V(r,\varphi,\lambda) \qquad \sum_{\ell=2}^{\infty} \sum_{m=0}^{\ell} \frac{\mu_\oplus}{r} \left(\frac{R_\oplus}{r}\right)^{\ell} \bar{P}_{\ell m}(\sin\varphi)[\bar{C}_{\ell m} \cos m\lambda + \bar{S}_{\ell m} \sin m\lambda] \; . \tag{27}$$

It is possible to deduce analytic expressions for all the gradient components, but for simplicity and since it will later be assumed that only Γ_{rr} is measured, an expression for Γ_{rr} will suffice here. (Actually there are six pieces of information available.)

$$\Gamma_{rr} \qquad \sum_{\ell=2}^{\infty} \sum_{m=0}^{\ell} (\ell+1)(\ell+2) \frac{\mu_\oplus}{r^3} \left(\frac{R_\oplus}{r}\right)^{\ell} \bar{P}_{\ell m}(\sin\varphi) [\bar{C}_{\ell m} \cos m\lambda + \bar{S}_{\ell m} \sin m\lambda] \; . \tag{28}$$

An important point to be noted in (28) is that although the entire gravity gradient tensor at a point cannot be reconstructed with just Γ_{rr}, it is possible to deduce values for all the tesseral harmonic coefficients with just Γ_{rr} (or in fact, with any single tensor component). In fact, the measurement $z = \Gamma_{rr}(r, \varphi, \lambda) + v$ is <u>linear</u> in the harmonic coefficients (with white noise v added) and so the whole theory of linear least-squares estimation theory can be applied. Letting the state vector x contain all tesseral harmonic coefficients,

$$z = Hx + v \tag{29}$$

where

$$H^T = \begin{bmatrix} (\ell+1)(\ell+2)\left(\frac{\mu_\oplus}{r^3}\right)\left(\frac{R_\oplus}{r}\right)^{\ell} \bar{P}_{\ell m}(\sin\varphi)\cos m\lambda \\ (\ell+1)(\ell+2)\left(\frac{\mu_\oplus}{r^3}\right)\left(\frac{R_\oplus}{r}\right)^{\ell} \bar{P}_{\ell m}(\sin\varphi)\sin m\lambda \\ \vdots \end{bmatrix}$$

$$x^T = [\bar{C}_{22},\ \bar{S}_{22},\ \bar{C}_{32},\ \bar{S}_{32},\ \ldots \\ \bar{C}_{33},\ \bar{S}_{33},\ \bar{C}_{43}\ \ \bar{S}_{43},\ \ldots] \ ,$$

and successive rows of H^T are formed with increasing values of ℓ and m. For satellite coverage of sufficiently large portions of the earth, the information matrix (inverse of the covariance matrix) can be approximated as

$$I_{ij} = \sum_K \frac{H_i(r,\varphi,\lambda_K)\ H_j(r,\varphi,\lambda_K)}{R} \tag{30}$$

since R is a scalar; (30) makes use of the fact that the satellite is in a polar orbit, and hence, latitude coverage is continuous, while longitude coverage is discrete.

$$I_{ij} \approx \int_0^{2\pi} (\ell+1)(\ell+2)(\ell'+1)(\ell'+2)\left(\frac{\mu_\oplus}{r^3}\right)^2\left(\frac{R_\oplus}{r}\right)^{\ell+\ell'} \cdot \bar{P}_{\ell m}(\sin\varphi)\,\bar{P}_{\ell' m'}(\sin\varphi) \cdot \begin{Bmatrix}\cos m\lambda \\ \sin m\lambda\end{Bmatrix}\begin{Bmatrix}\cos m'\lambda \\ \sin m'\lambda\end{Bmatrix} \frac{\cos\varphi\, d\varphi}{R\Delta\varphi} \quad (31)$$

Unless $m = m'$, then with sufficient coverage $I_{ij} = 0$, so harmonics with different m decouple and the only remaining problem is

$$I_{ij} \approx \int_0^{2\pi} (\ell+1)(\ell+2)(\ell'+1)(\ell'+2)\left(\frac{\mu_\oplus}{r^3}\right)^2\left(\frac{R_\oplus}{r}\right)^{\ell+\ell_1} \bar{P}_{\ell m}(\sin\varphi)\bar{P}_{\ell' m}(\sin\varphi)\begin{Bmatrix}\cos^2 m\lambda \\ \sin^2 m\lambda\end{Bmatrix}\cos\varphi\, d\varphi \quad (32)$$

where T is the correlation time of the measurement noise in units of radians of orbit. Rewriting (32), we have

$$I_{ij} = \frac{(\ell+1)(\ell+2)(\ell'+1)(\ell'+2)}{2RT}\left(\frac{\mu_\oplus}{r^3}\right)^2\left(\frac{R_\oplus}{r}\right)^{\ell+\ell'}\begin{Bmatrix}\cos^2 m\lambda \\ \sin^2 m\lambda\end{Bmatrix}\int_0^{2\pi} \bar{P}_{\ell m}(\sin\varphi)\bar{P}_{\ell' m}(\sin\varphi)\cos\varphi\, d\varphi \quad (33)$$

Unless $\ell = \ell'$ the integral in (33) is zero. When $\ell = \ell'$, the value of the integral is

$$\frac{2}{(2 - \delta_{0m})}$$

so I_{ij} is diagonal and the elements are

$$I_{kk} = \frac{(\ell+1)^2(\ell+2)^2}{2RT}\left(\frac{\mu_\oplus}{r^3}\right)^2\left(\frac{R_\oplus}{r}\right)^{2\ell}\frac{1}{2}\frac{2}{(2 - \delta_{0m})} \quad (34)$$

where the average value of $\sin^2$ and $\cos^2$ is taken to be $\frac{1}{2}$. The

information matrix for the $\bar{C}_{\ell m}$ and $\bar{S}_{\ell m}$ has diagonal elements

$$(\ell+1)^2(\ell+2)^2\, n^4 \left(\frac{R_\oplus}{r}\right)^{2\ell} \frac{\#\ \text{orbits}}{\pi} \frac{1}{2RT} \frac{2}{2-\delta_{0m}} \tag{35}$$

where

$$n^2 = \left(\frac{\mu_\oplus}{r^3}\right) .$$

This gives the $\sqrt{\text{variance}}$ for a particular $\bar{C}_{\ell m}$ or $\bar{S}_{\ell m}$ of

$$\sigma_{\bar{J}_{\ell m}} = \sqrt{\frac{2\pi RT}{\#\ \text{orbits}}} \left(\frac{r}{R_\oplus}\right)^2 \frac{1}{n^2(\ell+1)(\ell+2)} . \tag{36}$$

Again, using Kaula's rule of thumb,

$$\bar{J}_{\ell m} = \frac{14.14}{\ell^2} \times 10^{-6} .$$

So,

$$\frac{\sigma_{\bar{J}_{\ell m}}}{\bar{J}_{\ell m}} = \sqrt{\frac{2\pi\ RT}{\#\ \text{orbits}}} \left(\frac{r}{R_\oplus}\right)^{\ell} \frac{1}{n^2} \times \frac{10^6}{14.14} . \tag{37}$$

Now

n^2 = 3000 E

T = 10 sec $\cong$ 0.0116 rad

R = 0.1 E

orbit = 3 months $\cong$ 1200 orbits.

Figure 4 shows a comparison of various three-month geodesy missions, including the current knowledge, counter orbiting satellites (C.O.), gravity gradiometers (G.G.) at different altitudes, and satellite-to-satellite (S-S) tracking.

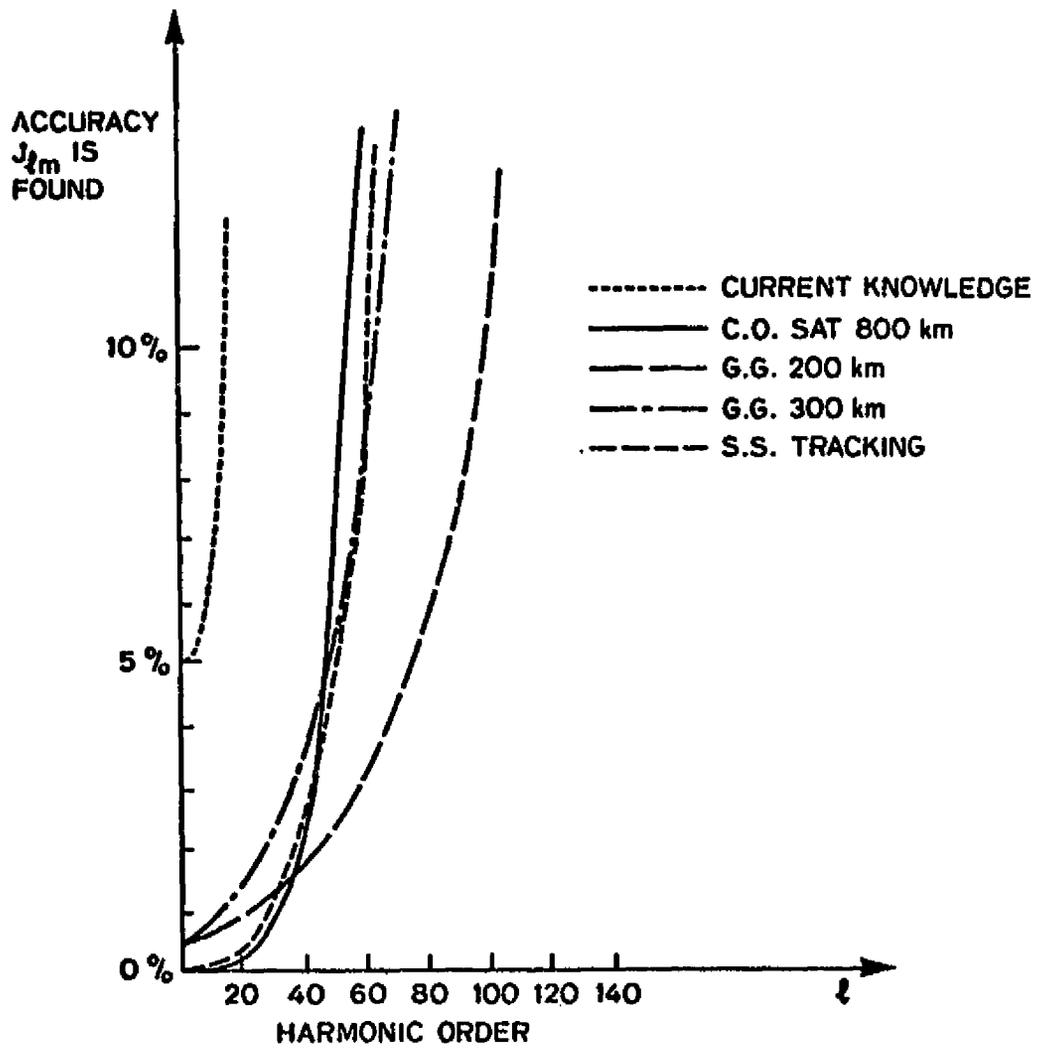

FIG. 4 A COMPARISON OF VARIOUS THREE-MONTH MISSIONS.

Due to the fact that the gradiometer yields a derivative measurement, it tends to amplify the high frequency components of the earth's gravity field. This is evident in Fig. 4. The gradiometer outperforms the various other experiments in the high harmonic range.

Chapter V

KALMAN FILTERING FOR GRAVITY GRADIOMETER AUGMENTING INERTIAL NAVIGATION SYSTEMS

A. INTRODUCTION

Inertial navigation is based on the simple principle that position is given by the double integration of acceleration. Accelerometers do not measure accelerations themselves but measure specific forces which are defined as all forces acting per unit mass with the exception of the gravity force. Hence, in order to obtain true accelerations, the specific force due to the gravity must be subtracted from the outputs of the accelerometers, in other words, the gravity acceleration must be added:

$$\bar{\alpha} = \bar{f} + \bar{g} \tag{38}$$

where

$\bar{\alpha}$ = acceleration of the vehicle

$\bar{f}$ = specific force

$\bar{g}$ = gravity acceleration of the earth.

Current inertial navigation systems use a "reference ellipsoid model" to compute the gravity acceleration of the earth, given the vehicle position. Although the reference ellipsoid model can well approximate the real gravity field of the earth, the difference is becoming a major error source of inertial navigation systems because of rapid hardware technology advances with accelerometers and gyroscopes [11].

The difference between the actual gravity and the reference ellipsoid model may be expressed in terms of gravity anomaly (magnitude) and deflections of the vertical (angular deviation), [12].

From measurements taken at 12.5 nm intervals across the 35th parallel in the United States, the standard deviation and the correlation distance of the vertical deflection were determined as 5.2 arcseconds and 25.1 n mi, respectively [Gelb, A.1974]. The worldwide vertical deflection ensemble is considered to have 8 arcsecond rms and 20 n mi correlation distance [13].

Compensation for the errors caused by the gravity deflection and anomaly is one of the principal applications of gravity gradiometers currently under development. Gravity gradiometers measure gravity gradients which are related to gravity acceleration by the following relation:

$$\frac{d\bar{g}}{dt} = \bar{\bar{\Gamma}} \cdot \bar{v} \tag{39}$$

where

$\bar{\bar{\Gamma}}$ = gravity gradient tensor of the earth

$\bar{v}$ = velocity of the vehicle.

Given the gravity gradients with the velocity and the initial values of the gravity, we can integrate (39) to obtain the gravity. However, as is well known, bias errors of the gravity gradiometers may produce unbounded position errors as time increases. This fact is easily seen by the following simple example illustrated in Fig. 5. Assuming that only error source is the bias of the gr diometer, the linearized error propagation equation for a single horizontal channel with constant speed may be given by

$$\Delta\dot{x} = \Delta v \tag{40a}$$

$$\Delta\dot{v} = \Delta g_x \tag{40b}$$

$$\Delta\dot{g}_x = v\Delta\Gamma_{xx} + \Gamma_{xx}\Delta v \tag{40c}$$

where

Δx, Δv and Δg_x = estimation errors of position, velocity and gravity disturbance, respectively

$b = \Delta\Gamma_{xx}$ = bias error of the gradiometer.

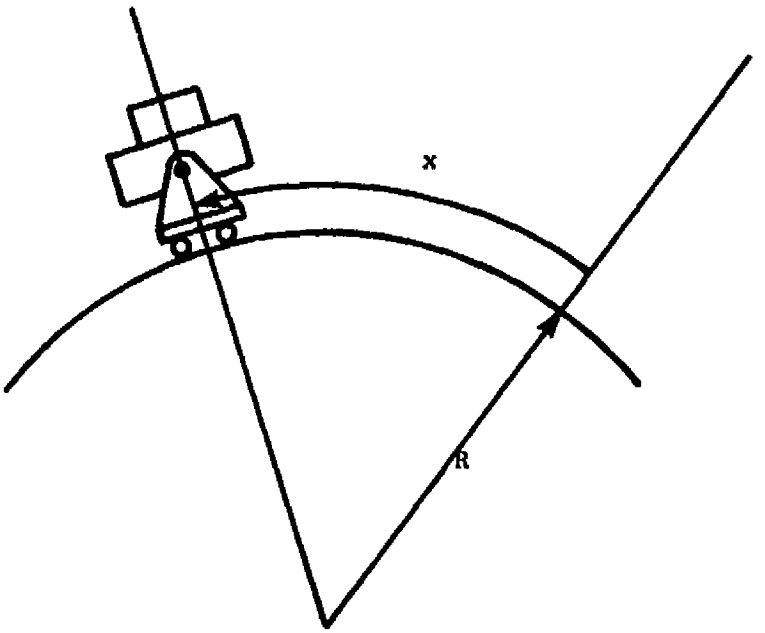

(a) Schematic

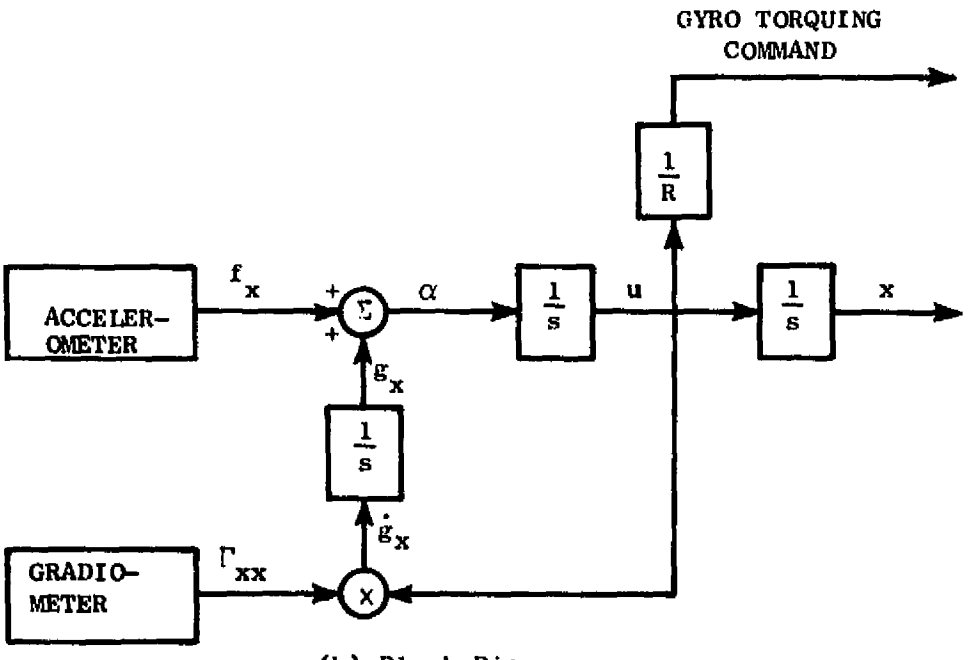

(b) Block Diagram

FIG. 5 A SINGLE HORIZONTAL INERTIAL NAVIGATION SYSTEM WITH A GRAVITY GRADIOMETER.

For the spherical earth, the value of Γ_{xx} is constant and equal to $-\frac{g}{R} \cong -1400$ E. where R is the radius of the earth. Substituting $-\frac{g}{R}\left(\triangleq\omega_s^2\right)$ for Γ_{xx}, we can integrate (40) to yield

$$\Delta x = \frac{vb}{\omega_s^2} t + \frac{A}{\omega_s} \cos(\omega_s t + \phi) \tag{41a}$$

$$\Delta v = \frac{vb}{\omega_s^2} + A \sin(\omega_s t + \phi) \tag{41b}$$

$$\Delta g_x = A\omega_s \cos(\omega_s t + \phi) \tag{41c}$$

where A and ϕ are constants determined by

$$\frac{vb}{\omega_s^2} + A \sin \phi = \Delta v_0 = \text{initial velocity error}$$

$$A\omega_s \cos \phi = \Delta g_{x0} = \text{initial gravity error.}$$

Equation (41a) indicates that the position error due to the bias of the gradiometer becomes unbounded with increasing time.

In order to overcome this difficulty, Heller [13] proposed a method of using gravity gradiometer as an external aid combined with a gravity deflection model. He obtained a number of numerical results for a single horizontal channel, assuming velocity reference errors, accelerometer errors, and gradiometer errors.

In the following sections, we try to obtain an analytical solution for Heller's mechanization, considering the gradiometer error as the only error source. Then, we extend his mechanization to estimate the bias error of the gradiometer (the bias error in this case means the difference of the means of the outputs of the gradiometer from the gravity deflection model).

B. SOLUTION FOR A SINGLE HORIZONTAL CHANNEL

The mechanization considered here is the same as "Gradiometer-as-an-external aid" (GAEA) in Heller [13], see Fig. 6. The gravity obtained

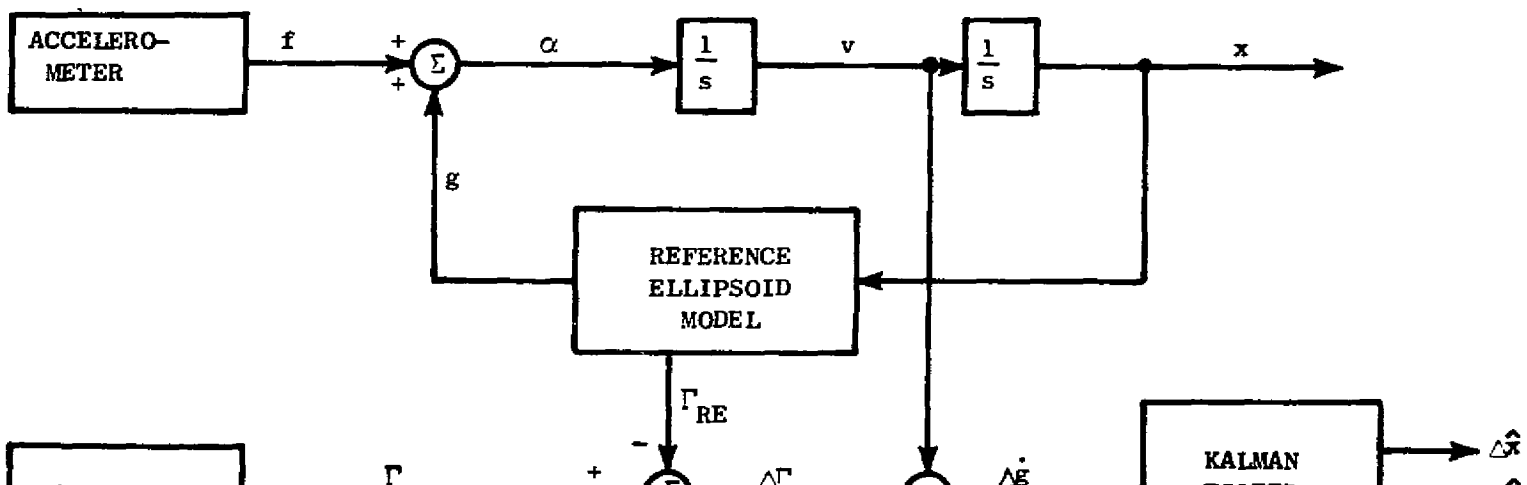

FIG. 6 GRADIOMETER AS AN EXTERNAL NAVIGATION AID (GAEA) [from Heller 1975]

by the reference ellipsoid is used for navigation computation. External velocity information is provided in feedback form in order to damp the Schuler oscillation. Gradiometer measurements are combined with a gravity deflection model to estimate the navigation errors via use of a Kalman filter. The vehicle speed is assumed to be constant.

Among various statistical gravity deflection models [Ref. 15], we choose the second order Markov model which is suitable for Kalman filter implementation because the governing equations may be written in the form of linear differential equations given by

$$\begin{aligned} \dot{g\xi} &= -\beta g\xi + \beta g\xi' \\ \dot{g\xi'} &= -\beta g\xi' + \beta W_\xi \end{aligned} \tag{42}$$

where

ξ = vertical deflection

ξ' = augmented state

β = Markov parameter

W_ξ = zero mean white noise with power spectral density q_ξ.

β and q_ξ are given by

$$\begin{aligned} \beta &= \frac{2.146v}{D} \\ q_\xi &= \frac{4g^2\xi_{rms}^2}{\beta} \end{aligned} \tag{43}$$

where D and ξ_{rms} are the correlation distance and rms of the vertical deflection respectively.

In this section, we consider that the gradiometer error is described by a zero mean white noise. Then the measurement equation may be approximated by

$$\begin{aligned} Z = v(\Gamma_{xx} - (\Gamma_{xx})_{RE}) &= \dot{g\xi} + vV_g \\ &= -\beta g_\xi + \beta g\xi' + vV_g \end{aligned} \tag{44a}$$

where

Γ_{xx} = output of gradiometer

$(\Gamma_{xx})_{RE} = \Gamma_{xx}$ computed by using the reference ellipsoid model

V_g = zero mean white noise of the gradiometer with power spectral density V_g.

V_g is given by

$$V_g = T\Delta\Gamma_g^2 \tag{44b}$$

where

T = averaging time

$\Delta\Gamma_g$ = rms of gradiometer error.

For simplicity, and to make clear the effect of the gravity deflection, we assume that the only position error source is due to gravity deflection. Then, the error propagation equation for a single horizontal channel may be written as

$$\begin{aligned} \Delta\dot{x} &= \Delta v \\ \Delta\dot{v} &= -\omega_s^2\Delta x - 2\zeta\omega_s\Delta v + g_\xi \end{aligned} \tag{45}$$

where

ζ = external velocity damping coefficient

$\omega_s \triangleq \frac{g}{R}$ = Schuler angular frequency.

As is clearly seen, the gravity deflection, ξ, and its augmented state ξ' are observable by the gradiometer measurement, but the navigation errors in position (Δx) and velocity (Δv) are not observable. Hence, we can construct Kalman filter for ξ and ξ' and have the best estimates $\hat{\xi}$ and $\hat{\xi}'$ given by

$$\begin{aligned} \dot{g\hat{\xi}} &= -\beta g\hat{\xi} + g\hat{\xi}' + K_\xi(Z + v\beta g\hat{\xi} - v\beta g\hat{\xi}') \\ g\dot{\hat{\xi}}' &= -\beta g\hat{\xi}' + K_{\xi'}(Z + v\beta g\hat{\xi} - v\beta g\hat{\xi}') \end{aligned} \tag{46}$$

where K_{ξ} and $K_{\dot{\xi}}$ are Kalman filter gains.

Now, the estimation error in gravity disturbance, $g_{\xi}-g_{\xi}'$, drives the error equation (45), rather than the full gravity disturbance, g_{ξ}.

The Kalman filter for the gravity deflection and its augmented state may be found as follows. First, the transfer function from the process noise w_{ξ} to the measurement z may be found as

$$\frac{z}{w_{\xi}} = \frac{\beta^2 s}{(s+\beta)^2} \cdot \tag{47}$$

Then, the symmetric root characteristic equation may be written by

$$1 + \frac{\beta^2 s}{(s+\beta)^2} \frac{q_{\xi}}{v^2 V_g} \frac{(-\beta^2 s)}{(-s+\beta)^2} = 0 \tag{48a}$$

or

$$1 + \frac{s^*}{(s^*+1)^2} (2a)^2 \frac{(-s^*)}{(-s^*+1)^2} = 0 \tag{48b}$$

where

$$s^* \triangleq \frac{s}{\beta} \tag{48c}$$

$$a \triangleq \frac{\beta}{2v} \sqrt{\frac{q_{\xi}}{V_g}} = \sqrt{\frac{2.146}{DVT}} \frac{g^{\xi}_{rms}}{\sqrt{\Gamma_g}} \cdot \tag{48d}$$

The symmetric root locus with parameter a may be readily drawn as shown in Fig. 7. In this case, we can solve the characteristic equations (48) and obtain the roots

$$s^* = \pm a \pm \sqrt{1+a^2} \tag{49}$$

we also find the steady-state Kalman filter gains given by

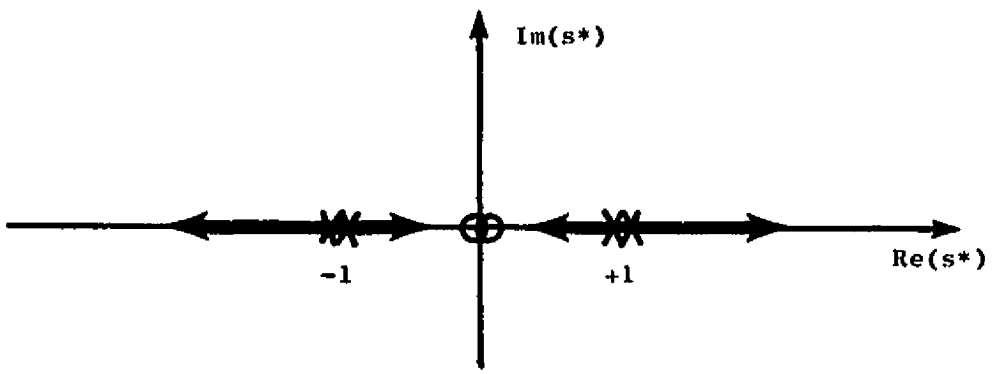

FIG. 7 NORMALIZED SYMMETRIC ROOT LOCUS

$$K_\xi = 0$$

$$K_{\xi'} = 2\left(\sqrt{1+a^2} - 1\right) . \tag{50}$$

The covariance of the estimation error of the gravity deflection $P_{\xi\xi}$ is given by

$$P^*_{\xi\xi} \triangleq \frac{P_{\xi\xi}}{\left(\frac{\beta q_\xi}{4}\right)} = \frac{2\left(\sqrt{1+a^2} - 1\right)}{a^2} . \tag{51}$$

As the accuracy of the gradiometer improves ($\Delta\Gamma_g \to 0$ or $a \to \infty$), the error covariance $P^*_{\xi\xi}$ decreases monotonically (Fig. 8). For example, for ξ_{rms} = 8 arcsec, D = 20 n mi, and v = 100 knots, we have from (43)

$$\beta = 10.73 \ (hr^{-1})$$

$$q_\xi = 2.91 \ (n.mi^2 \ hr^{-3}) .$$

For T = 10 sec, $\Delta\Gamma g$ = 1E, we have from (44b)

$$V_g = 4.67 \times 10^{-7} (hr^{-3}) .$$

Hence, from (48d) and (51), we have

$$a = 134$$

$$P^*_{\xi\xi} = .0148 .$$

The rms of the estimation error in the vertical deflection decreases to about one tenth of that without the gradiometer. However, as $a \to \infty$, one characteristic root approaches the origin and the other approaches infinity. This fact indicates that the gravity deflection is obtained by integration of the measurement, ignoring the gravity deflection model.

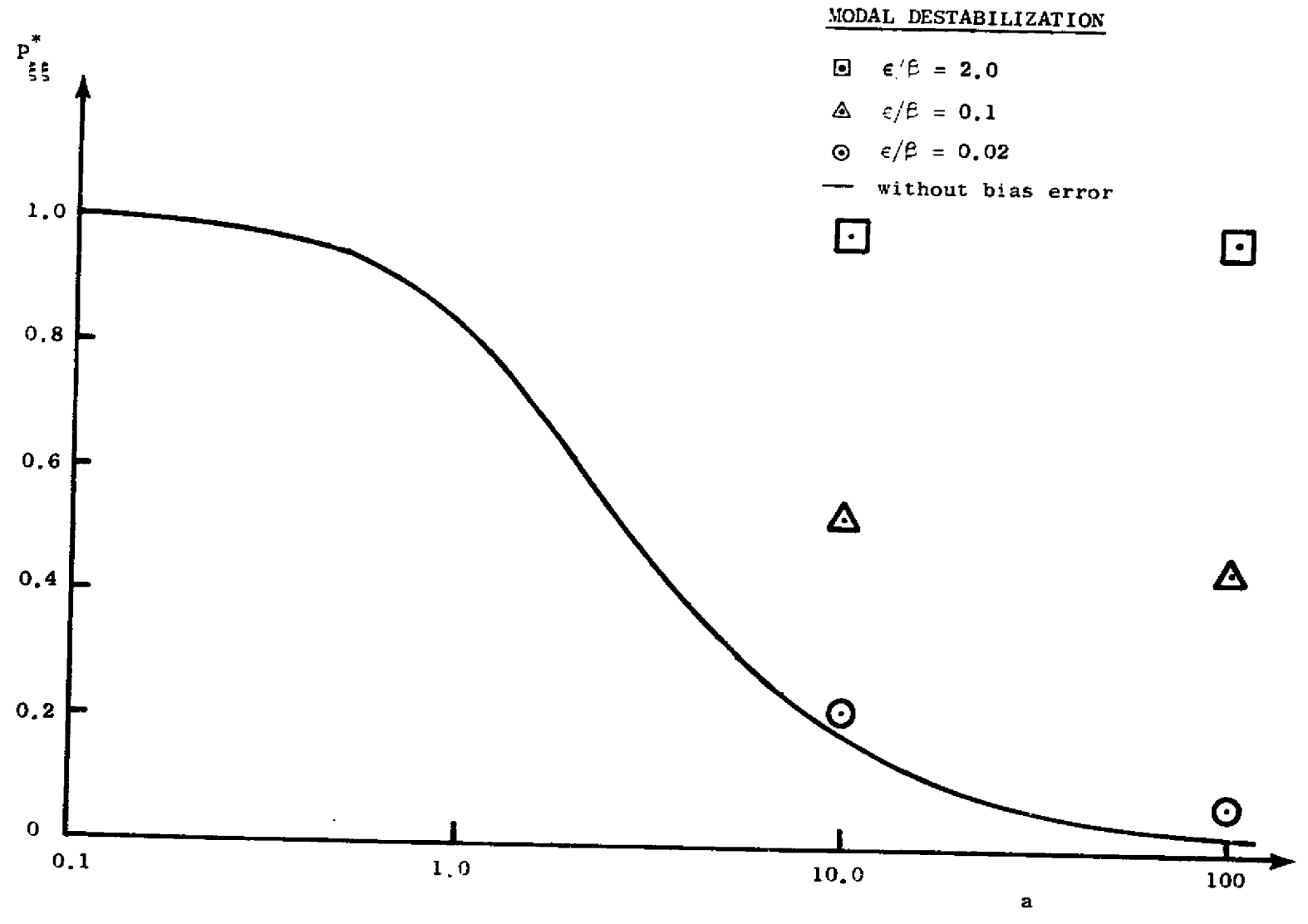

FIG. 8 NORMALIZED COVARIANCE OF VERTICAL DEFLECTION ESTIMATION ERROR.

Substituting the estimation error of the gravity deflection $\xi-\hat{\xi}$ for ξ in (45b) and conducting tedious calculation, we have expressions for the covariance of errors in position (P_{xx}) and velocity (P_{vv}) given by

$$P^*_{xx} \triangleq \frac{P_{xx}}{(P_{xx})_0} = \frac{2(\sqrt{1+a^2}-1)\left(\zeta\omega_s^{*3} + 4\zeta^2\sqrt{1+a^2}\,\omega_s^{*2} + 4\zeta(1+a^2)\omega_s^* + \sqrt{1+a^2}\right)\Delta_0^*}{a^2(\zeta\omega_s^{*3} + 4\zeta^2\omega_s^{*2} + 4\zeta\omega_s^* + 1)\Delta^*} \tag{52a}$$

$$P^*_{vv} \triangleq \frac{P_{vv}}{(P_{vv})_0} = \frac{2(\sqrt{1+a^2}-1)\,(\zeta\omega_s^* + \sqrt{1+a^2})\,\Delta_0^*}{a^2(\zeta\omega_s^* + 1)\,\Delta^*} \tag{52b}$$

where

$(P_{xx})_0$, $(P_{vv})_0$ = covariances of errors in position and velocity, without gradiometer measurement

$$\Delta^* = \omega^{*4} + 4\zeta\sqrt{1+a^2}\,\omega_s^{*3} + (4\zeta^2+4a^2+2)\omega_s^{*2} + 4\zeta\sqrt{1+a^2}\,\omega_s^* + 1$$

$$\Delta_0^* = (\omega_s^{*2} + 2\zeta\omega_s^* + 1)^2$$

$$\omega_s^* = \omega_s/\beta\,.$$

Among numerical examples shown in Figs. 9, the case with the vehicle velocity 1000 knots is particularly interesting because when the root mean square values of the gravity gradiometer error are around 10 E, the covariances of position and velocity errors become larger than those without gradiometers. This fact suggests studying the power spectral density of the estimation error of the gravity deflection which is given by

$$\frac{(PSD)_{\tilde{g\xi}}}{q_\xi} = \frac{2\sqrt{1+a^2}\left(\sqrt{1+a^2}-1\right)}{a^2}\,\frac{1}{\omega^{*4} + 2(1+2a^{*2})\omega^{*2} + 1} \tag{53}$$

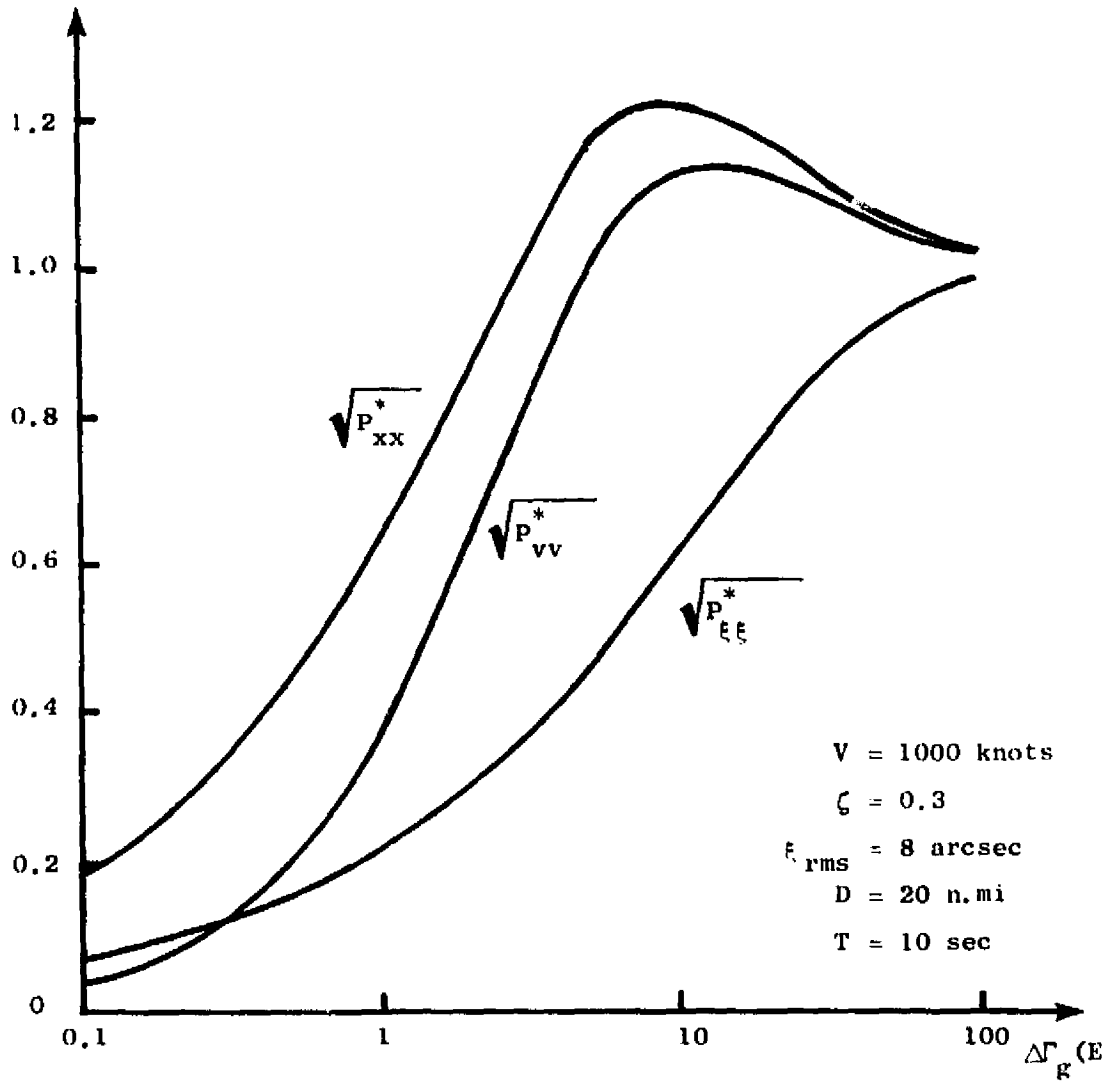

FIG. 9a NORMALIZED RMS VALUES OF ESTIMATION ERRORS IN POSITION, VELOCITY, AND VERTICAL DEFLECTION.

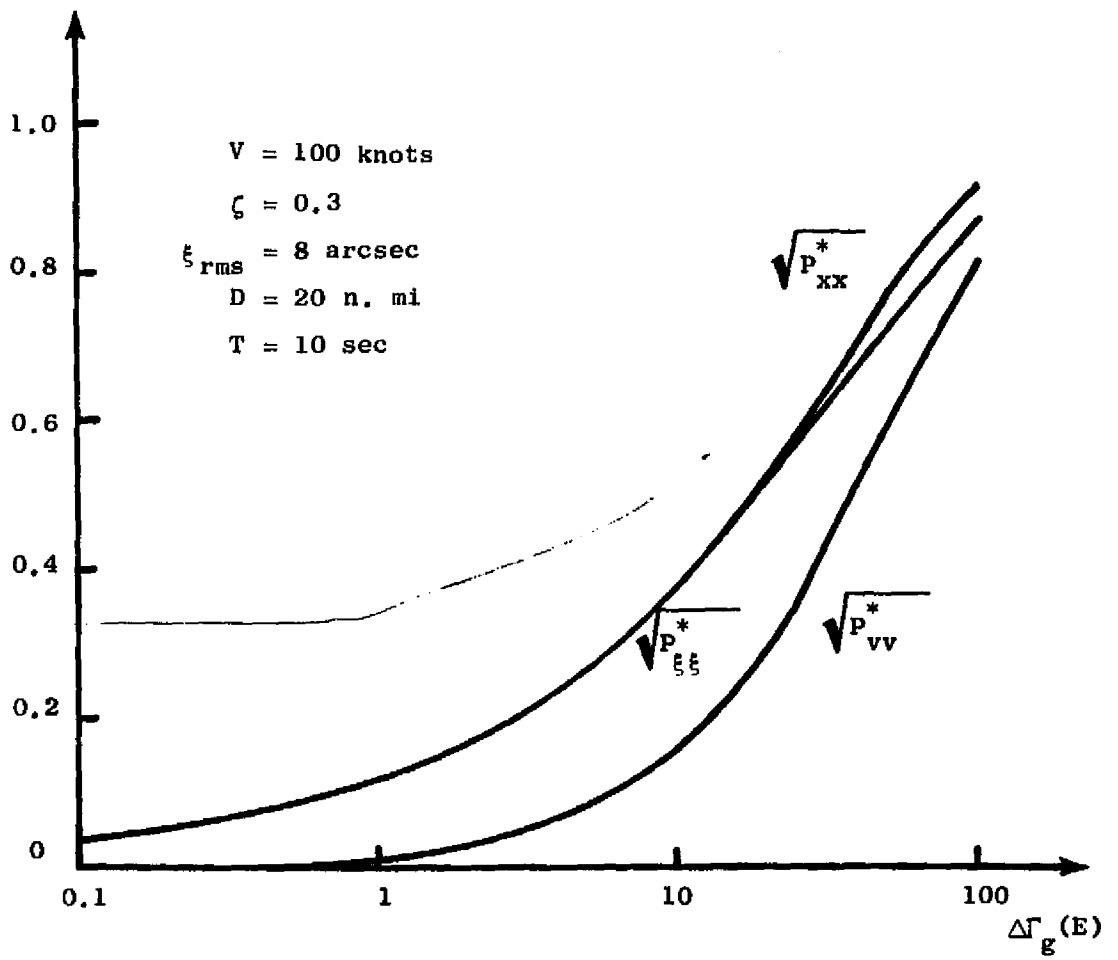

FIG. 9b NORMALIZED RMS VALUES OF ESTIMATION ERRORS IN POSITION, VELOCITY, AND VERTICAL DEFLECTION.

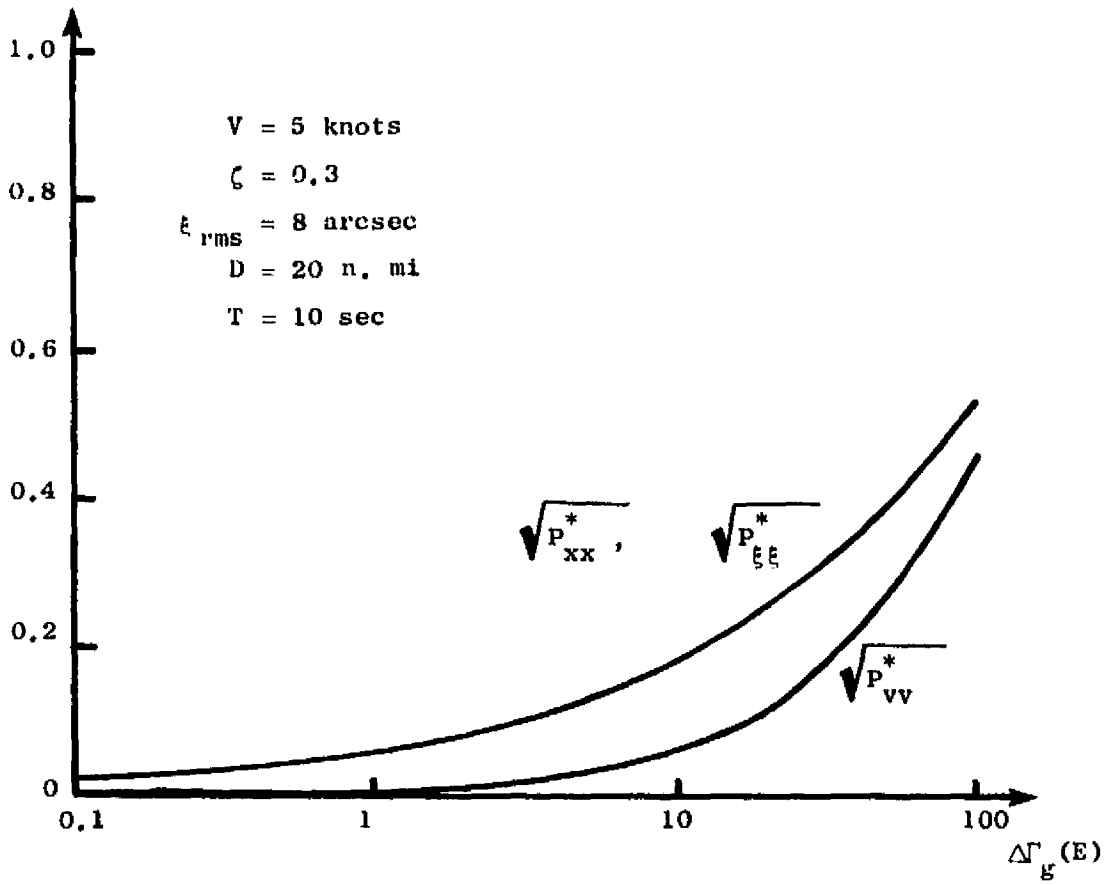

FIG 9c NORMALIZED RMS VALUES OF ESTIMATION ERRORS IN POSITION, VELOCITY, AND VERTICAL DEFLECTION.

where

$$\omega^* \triangleq \frac{\omega}{\beta} .$$

Examining (53) and Fig. 10a we find that near zero frequency the power spectral density of the estimation error of the gravity deflection is always larger (up to a factor of 2) than q_ξ. This means that even if the Kalman filter gives a smaller covariance as shown in Fig. 8, it does not give improved information near zero frequency, but worse. Hence, when the power spectral density of the gravity deflection error at Schuler frequency is larger than q_ξ, the covariances of position and velocity errors are larger with gradiometers than without.

C. BIAS ESTIMATE

In this section, we make an attempt to extend Heller's mechanization to estimate the bias error of the gradiometer, introducing the bias as an augmented state in the Kalman filter discussed in the previous section. The bias error in this case means the difference between the means of the outputs of the gradiometers and the gravity deflection model.

The measurement equation (44) may be rewritten as

$$Z = -\beta g\xi + \beta g\xi' + vb + vVg \tag{54}$$

where b is the bias error of the gradiometer and the additional state equation is simply

$$\dot{b} = 0 \tag{55}$$

The full system consists of equations (42), (54) and (55). Direct application of the Kalman filter theory to this problem fails, however. Since the bias is an undisturbable and neutrally stable mode, the Kalman filter gain associated with this mode becomes zero after the initial uncertaintly disappears. This is a typical example of Kalman filter divergence. Many cures have been proposed for this difficulty such as restarting, minimum

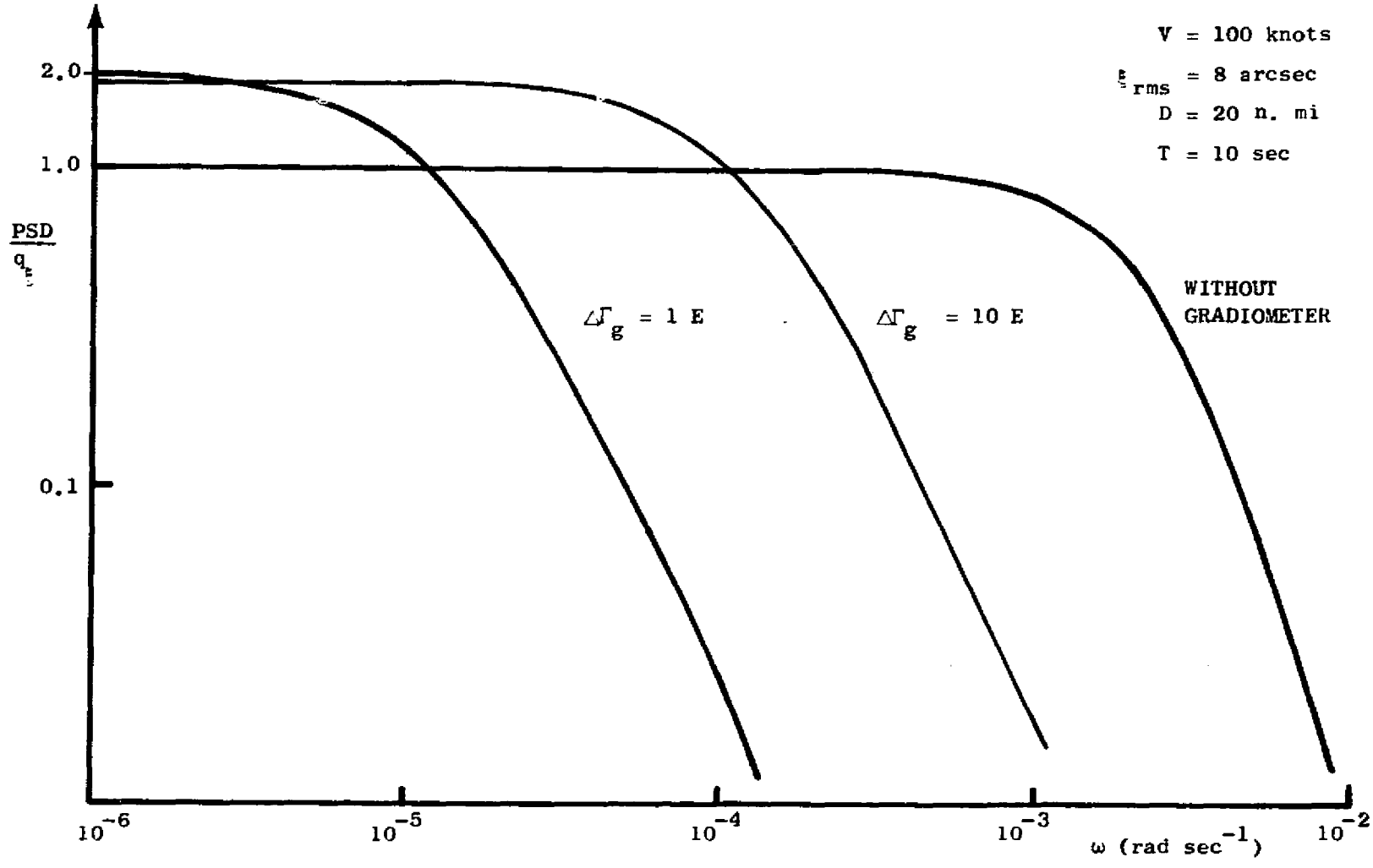

FIG. 10a POWER SPECTRAL DENSITY OF ESTIMATION ERROR OF VERTICAL DEFLECTION

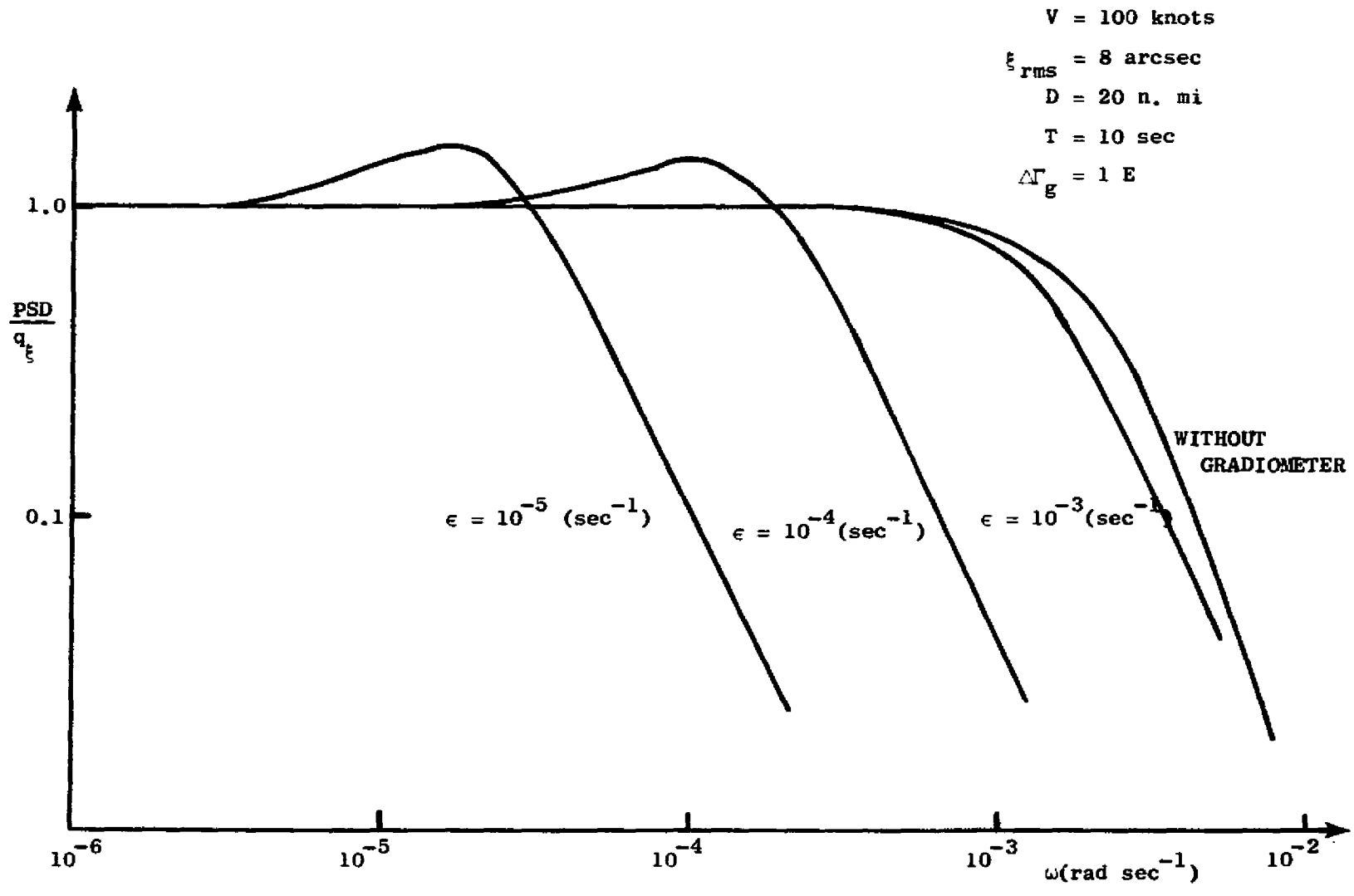

FIG. 10b POWER SPECTRAL DENSITY OF ESTIMATION ERROR OF VERTICAL DEFLECTION (Modal Destabilization).

variance observers with eigenvalue constraints, added noise, pole-shifting and destabilization which are discussed in Bryson [14]. Here, we use the modal destabilization method which is based on the fact that the steady-state Kalman filter for a system with an (undisturbed) unstable mode is stable. As the amount of destabilization increases, the absolute value of the eigenvalue associated with the undisturbed model increases from zero. However, the covariance of the estimation errors increases too. Some numerical results are shown in Fig. 8 and Table 1. The power spectral density of the estimation error of the gravity deflection was computed numerically and shown in Fig. 10b. Although there is still a hump higher than the original value q_ξ, the power spectral density of

Table 1

SOME NUMERICAL RESULTS OF SUBOPTIMAL FILTER OBTAINED BY MODAL DESTABILIZATION METHOD

a	ϵ/β	EIGENVALUES OF SUBOPTIMAL FILTER MEASURED IN UNITS OF β	$\frac{P_{\xi\xi}}{(\beta/4)\, q_\xi}$
100	0.001	−200.0 −0.004, −0.003	0.0243
	0.01	−200.0 −0.125 ± j0.012	0.073
	0.1	−200.0 −0.102 ± j0.084	0.451
	2.0	−20.0 −0.527, −1.694	0.979
10	0.001	−20.0 −0.050, −0.004	0.180
	0.01	−20.0 −0.042, −0.028	0.218
	0.1	−20.0 −0.124 ± j0.098	0.526
	2.0	−21.9 −0.556, −1.650	0.985

Chapter VI

ESTIMATION OF DISTRIBUTED MASS DENSITY

We have been trying a completely different way of processing gradiometer measurement from that discussed in the previous chapter. Instead of equation (39), we use the gradiometer measurement to estimate the mass density distribution of the earth, then compute the gravity from the density distribution. This approach not only brings up a very interesting problem, i.e., filtering of a distributed system, but also seems to have the following practical advantages:

(a) The bias of the gradiometer does not cause an unbounded position error but, at most, excites the Schuler oscillation. This is because both the gravity and the gravity gradients are obtained by spatial integration of the mass density and time-integration of the gradiometer measurement is not needed.

(b) Since the statistical model of the mass density distribution is needed only at the boundary, the effect of the model error is small. Furthermore, there is little difficulty in extending this approach to the actual inhomogeneous earth density field.

On the other hand, obviously this method requires large computer capacity. However, since the correlation distance of the gravity deflection is about twenty nautical miles, we do not have to estimate the density distribution over large areas for inertial navigation purposes. This fact may relax the requirement of the computer capacity.

So far, we have derived the partial differential equation for the density distribution and obtained the filtering algorithm, including distributed Kalman filter gain. Numerical calculation is in progress.

Chapter VII

CONCLUSIONS AND RECOMMENDATIONS FOR FURTHER STUDY

Several gravity models, including

1) tesseral harmonic models
2) point mass and line mass models
3) second order random process models

have been studied. As a result of the fact that inertial navigators are particularly sensitive to what happens locally, it could be proved rigorously that the tesseral harmonic model probably could never be implemented due to the large number of parameters needed to obtain a suitably accurate local gravity description.

The second order random process model was studied in detail. We obtained an analytical solution for Heller's mechanization (GAEA), using a more simplified problem formulation which still retains the part essential for gradiometer study. The solution shows that the covariances of the errors in position and velocity are larger than those without gradiometer when Schuler frequency falls within the bandwidth of the estimation error in the vertical deflection.

We extended Heller's Kalman filter to estimate the bias error of the gradiometer, using the modal destabilization method to avoid Kalman filter divergence.

Point mass and line mass models still should be considered, due to the simplicity with which they could be implemented. Future work will contain numerical results based on these models.

Recently, another method of obtaining gravity perturbations has come under consideration, the estimation of distributed mass density. At this point, the necessary analytical work has been completed, and future work will include numerical results.

The problem of bias estimation of the gravity gradiometer has now been studied in some detail. After several schemes were considered, the

most favorable methods to emerge are

1) If possible, retrace a given groundtrack with the gradiometer in three different orientations.
2) Calibrate the gravity gradiometer bias at a fixed location in many different orientations to obtain the bias accurately before the instrument is used as a system component.

Finally, the results of using a gravity gradiometer to perform a geodesy mission accurately are compared with competing schemes. A low orbiting gradiometer appears to be the most effective way of obtaining the tesseral harmonics of the earth for order 40 and above, i.e., the high frequency components. In the range below the 40th harmonic, the geodesy mission employing counter-orbiting drag free satellites is superior.

REFERENCES

1. Ames, C.B., R.L. Forward, et. al., "Prototype Moving Base Gravity Gradiometer;" R&D Design Evaluation Rept, Hughes Research Labs, Malibu, Calif., Jan 1973.

2. Metzger, E.H., and A. Jircitano, "Analysis of Real Time Mapping of Horizontal and Vertical Gravity Anomalies Aboard A Moving Vehicle Such as an Aircraft," Int'l Symposium on Application of Marine Geodesy, Columbus, Ohio, Jun 1974.

3. Trageser, M.B., "A Gradiometer System for Gravity Anomaly Surveying," from Advances in Dynamic Gravimetry, Proc. of the Symposium on Dynamic Gravimetry, (T. Kattner, editor), Fort Worth, Texas, Mar 1970.

4. Trageser, M.B., "Feasibility Model Gravity Gradiometer Test Results", AIAA Guidance & Control Conf., Boston, Mass, Aug 1975, paper No. 75-1093.

5. Metzger, E.H., 1977 AIAA Guidance & Control Conf., Florida, 1977.

6. DeBra, D.B., and E. Pelka, "Study to Develop Gradiometer Compensation Techniques," Final Report submitted to AFGL by the Guidance & Control Dept., Stanford University, Stanford, Ca., 94305, Dec. 1976.

7. Kaula, W., Theory of Satellite Geodesy, Blaisdell Press, Waltham, Mass, 1966.

8. Allan, R.R., "Resonance with Longitude Dependent Gravity," Planetary Space Sciences 1967, Vol. 15, pp. 53-76, 1967.

9. Bryson, A., and Y.C. Ho, Applied Optimal Control, Blaisdell Press, Waltham, Mass., p. 373, 1969.

10. ibid., p. 381.

11. Britting, K.R., Madden, S.J., and Hildebrant, R.A., "Assessment of the Impact of Gradiometer Techniques on the Performance of Inertial Navigation Sysemts," RE-78, Measurement System Lab. MIT, Cambridge, Mass., Sep 1971.

12. Heiskanen, W.E. and Montz, H., "Physical Geodesy," San Francisco: Freeman, 1967.

13. Heller, W.G., "Gradiometer-Aided Inertial Navigation," TR-312-5, The Analytic Science Corporation, Reading, Mass., 1975.

14. Bryson, A.E., "Kalman Filter Divergence and Aircraft Motion Estimators," SUDAAR 505, Stanford University, Stanford, Ca., 1977.

15. Jordan, S.K., "Effects of Geodetic Uncertainties On A Damped Inertial Navigation System," IEEE Vol. AES-9, No. 5, Sep 1973.

16. Gelb, A., edited, "Applied Optimal Estimation," MIT Press, 1974.